Eur. Phys. J. C 35, 487–500 (2004)
Digital Object Identifier (DOI) 10.1140/epjc/s2004-01885-2

THE EUROPEAN PHYSICAL JOURNAL C

The dependence of dijet production on photon virtuality in ep collisions at HERA

The ZEUS Collaboration

S. Chekanov, M. Derrick, J.H. Loizides[1], S. Magill, S. Miglioranzi[1], B. Musgrave, J. Repond, R. Yoshida
Argonne National Laboratory, Argonne, Illinois 60439-4815, USA[n]

M.C.K. Mattingly
Andrews University, Berrien Springs, Michigan 49104-0380, USA

N. Pavel
Institut für Physik der Humboldt-Universität zu Berlin, Berlin, Germany

P. Antonioli, G. Bari, M. Basile, L. Bellagamba, D. Boscherini, A. Bruni, G. Bruni, G. Cara Romeo, L. Cifarelli, F. Cindolo, A. Contin, M. Corradi, S. De Pasquale, P. Giusti, G. Iacobucci, A. Margotti, A. Montanari, R. Nania, F. Palmonari, A. Pesci, L. Rinaldi, G. Sartorelli, A. Zichichi
University and INFN Bologna, Bologna, Italy[e]

G. Aghuzumtsyan, D. Bartsch, I. Brock, S. Goers, H. Hartmann, E. Hilger, P. Irrgang, H.-P. Jakob, O. Kind, U. Meyer, E. Paul[2], J. Rautenberg, R. Renner, A. Stifutkin, J. Tandler[3], K.C. Voss, M. Wang
Physikalisches Institut der Universität Bonn, Bonn, Germany[b]

D.S. Bailey[4], N.H. Brook, J.E. Cole, G.P. Heath, T. Namsoo, S. Robins, M. Wing
H.H. Wills Physics Laboratory, University of Bristol, Bristol, United Kingdom[m]

M. Capua, A. Mastroberardino, M. Schioppa, G. Susinno
Calabria University, Physics Department and INFN, Cosenza, Italy[e]

J.Y. Kim, I.T. Lim, K.J. Ma, M.Y. Pac[5]
Chonnam National University, Kwangju, South Korea[g]

M. Helbich, Y. Ning, Z. Ren, W.B. Schmidke, F. Sciulli
Nevis Laboratories, Columbia University, Irvington on Hudson, New York 10027[o]

J. Chwastowski, A. Eskreys, J. Figiel, A. Galas, K. Olkiewicz, P. Stopa, L. Zawiejski
Institute of Nuclear Physics, Cracow, Poland[i]

L. Adamczyk, T. Bołd, I. Grabowska-Bołd[6], D. Kisielewska, A.M. Kowal, M. Kowal, J. Łukasik, M. Przybycień, L. Suszycki, D. Szuba, J. Szuba[7]
Faculty of Physics and Nuclear Techniques, AGH-University of Science and Technology, Cracow, Poland[p]

A. Kotański[8], W. Słomiński
Department of Physics, Jagellonian University, Cracow, Poland

V. Adler, U. Behrens, I. Bloch, K. Borras, V. Chiochia, D. Dannheim[9], G. Drews, J. Fourletova, U. Fricke, A. Geiser, P. Göttlicher[10], O. Gutsche, T. Haas, W. Hain, S. Hillert[11], C. Horn, B. Kahle, U. Kötz, H. Kowalski, G. Kramberger, H. Labes, D. Lelas, H. Lim, B. Löhr, R. Mankel, I.-A. Melzer-Pellmann, C.N. Nguyen, D. Notz, A.E. Nuncio-Quiroz, A. Polini, A. Raval, L. Rurua, U. Schneekloth, U. Stösslein, G. Wolf, C. Youngman, W. Zeuner
Deutsches Elektronen-Synchrotron DESY, Hamburg, Germany

S. Schlenstedt
DESY Zeuthen, Zeuthen, Germany

G. Barbagli, E. Gallo, C. Genta, P. G. Pelfer
University and INFN, Florence, Italy[e]

A. Bamberger, A. Benen, F. Karstens, D. Dobur, N.N. Vlasov

Fakultät für Physik der Universität Freiburg i.Br., Freiburg i.Br., Germany[b]

M. Bell, P.J. Bussey, A.T. Doyle, J. Ferrando, J. Hamilton, S. Hanlon, A. Lupi, D.H. Saxon, I.O. Skillicorn
Department of Physics and Astronomy, University of Glasgow, Glasgow, United Kingdom[m]

I. Gialas
Department of Engineering in Management and Finance, Univ. of Aegean, Greece

T. Carli, T. Gosau, U. Holm, N. Krumnack, E. Lohrmann, M. Milite, H. Salehi, P. Schleper, T. Schörner-Sadenius, S. Stonjek[11], K. Wichmann, K. Wick, A. Ziegler, Ar. Ziegler
Hamburg University, Institute of Exp. Physics, Hamburg, Germany[b]

C. Collins-Tooth, C. Foudas, R. Gonçalo[12], K.R. Long, A.D. Tapper
Imperial College London, High Energy Nuclear Physics Group, London, United Kingdom[m]

P. Cloth, D. Filges
Forschungszentrum Jülich, Institut für Kernphysik, Jülich, Germany

M. Kataoka[13], K. Nagano, K. Tokushuku[14], S. Yamada, Y. Yamazaki
Institute of Particle and Nuclear Studies, KEK, Tsukuba, Japan[f]

A.N. Barakbaev, E.G. Boos, N.S. Pokrovskiy, B.O. Zhautykov
Institute of Physics and Technology of Ministry of Education and Science of Kazakhstan, Almaty, Kazakhstan

D. Son
Kyungpook National University, Center for High Energy Physics, Daegu, South Korea[g]

K. Piotrzkowski
Institut de Physique Nucléaire, Université Catholique de Louvain, Louvain-la-Neuve, Belgium

F. Barreiro, C. Glasman[15], O. González, L. Labarga, J. del Peso, E. Tassi, J. Terrón, M. Zambrana
Departamento de Física Teórica, Universidad Autónoma de Madrid, Madrid, Spain[l]

M. Barbi, F. Corriveau, S. Gliga, J. Lainesse, S. Padhi, D.G. Stairs, R. Walsh
Department of Physics, McGill University, Montréal, Québec, Canada H3A 2T8[a]

T. Tsurugai
Meiji Gakuin University, Faculty of General Education, Yokohama, Japan[f]

A. Antonov, P. Danilov, B.A. Dolgoshein, D. Gladkov, V. Sosnovtsev, S. Suchkov
Moscow Engineering Physics Institute, Moscow, Russia[j]

R.K. Dementiev, P.F. Ermolov, I.I. Katkov, L.A. Khein, I.A. Korzhavina, V.A. Kuzmin, B.B. Levchenko, O.Yu. Lukina, A.S. Proskuryakov, L.M. Shcheglova, S.A. Zotkin
Moscow State University, Institute of Nuclear Physics, Moscow, Russia[k]

I. Abt, C. Büttner, A. Caldwell, X. Liu, J. Sutiak
Max-Planck-Institut für Physik, München, Germany

N. Coppola, S. Grijpink, E. Koffeman, P. Kooijman, E. Maddox, A. Pellegrino, S. Schagen, H. Tiecke, M. Vázquez, L. Wiggers, E. de Wolf
NIKHEF and University of Amsterdam, Amsterdam, Netherlands[h]

N. Brümmer, B. Bylsma, L.S. Durkin, T.Y. Ling
Physics Department, Ohio State University, Columbus, Ohio 43210[n]

A.M. Cooper-Sarkar, A. Cottrell, R.C.E. Devenish, B. Foster, G. Grzelak, C. Gwenlan[16], T. Kohno, S. Patel, P.B. Straub, R. Walczak
Department of Physics, University of Oxford, Oxford United Kingdom[m]

A. Bertolin, R. Brugnera, R. Carlin, F. Dal Corso, S. Dusini, A. Garfagnini, S. Limentani, A. Longhin, A. Parenti, M. Posocco, L. Stanco, M. Turcato
Dipartimento di Fisica dell' Università and INFN, Padova, Italy[e]

E.A. Heaphy, F. Metlica, B.Y. Oh, J.J. Whitmore[17]
Department of Physics, Pennsylvania State University, University Park, Pennsylvania 16802[o]

Y. Iga
Polytechnic University, Sagamihara, Japan[f]

G. D'Agostini, G. Marini, A. Nigro
Dipartimento di Fisica, Università 'La Sapienza' and INFN, Rome, Italy[e]

C. Cormack[18], J.C. Hart, N.A. McCubbin
Rutherford Appleton Laboratory, Chilton, Didcot, Oxon, United Kingdom[m]

C. Heusch
University of California, Santa Cruz, California 95064, USA[n]

I.H. Park
Department of Physics, Ewha Womans University, Seoul, Korea

H. Abramowicz, A. Gabareen, S. Kananov, A. Kreisel, A. Levy
Raymond and Beverly Sackler Faculty of Exact Sciences, School of Physics, Tel-Aviv University, Tel-Aviv, Israel[d]

M. Kuze
Department of Physics, Tokyo Institute of Technology, Tokyo, Japan[f]

T. Fusayasu, S. Kagawa, T. Tawara, T. Yamashita
Department of Physics, University of Tokyo, Tokyo, Japan[f]

R. Hamatsu, T. Hirose[2], M. Inuzuka, H. Kaji, S. Kitamura[19], K. Matsuzawa
Tokyo Metropolitan University, Department of Physics, Tokyo, Japan[f]

M. Costa, M.I. Ferrero, V. Monaco, R. Sacchi, A. Solano
Università di Torino and INFN, Torino, Italy[e]

M. Arneodo, M. Ruspa
Università del Piemonte Orientale, Novara, and INFN, Torino, Italy[e]

T. Koop, J.F. Martin, A. Mirea
Department of Physics, University of Toronto, Toronto, Ontario, Canada M5S 1A7[a]

J.M. Butterworth[20], R. Hall-Wilton, T.W. Jones, M.S. Lightwood, M.R. Sutton[4], C. Targett-Adams
Physics and Astronomy Department, University College London, London, United Kingdom[m]

J. Ciborowski[21], R. Ciesielski[22], P. Łużniak[23], R.J. Nowak, J.M. Pawlak, J. Sztuk[24], T. Tymieniecka, A. Ukleja, J. Ukleja[25], A.F. Żarnecki
Warsaw University, Institute of Experimental Physics, Warsaw, Poland[q]

M. Adamus, P. Plucinski
Institute for Nuclear Studies, Warsaw, Poland[q]

Y. Eisenberg, D. Hochman, U. Karshon M. Riveline
Department of Particle Physics, Weizmann Institute, Rehovot, Israel[c]

A. Everett, L.K. Gladilin[26], D. Kçira, S. Lammers, L. Li, D.D. Reeder, M. Rosin, P. Ryan, A.A. Savin, W.H. Smith
Department of Physics, University of Wisconsin, Madison, Wisconsin 53706, USA[n]

S. Dhawan
Department of Physics, Yale University, New Haven, Connecticut 06520-8121, USA[n]

S. Bhadra, C.D. Catterall, S. Fourletov, G. Hartner, S. Menary, M. Soares, J. Standage
Department of Physics, York University, Ontario, Canada M3J 1P3[a]

[1] also affiliated with University College London, London, UK
[2] retired
[3] self-employed
[4] PPARC Advanced fellow
[5] now at Dongshin University, Naju, South Korea
[6] partly supported by Polish Ministry of Scientific Research and Information Technology, grant no. 2P03B 12225
[7] partly supported by Polish Ministry of Scientific Research and Information Technology, grant no.2P03B 12625
[8] supported by the Polish State Committee for Scientific Research, grant no. 2 P03B 09322
[9] now at Columbia University, N.Y., USA

[10] now at DESY group FEB
[11] now at University of Oxford, Oxford, UK
[12] now at Royal Holoway University of London, London, UK
[13] also at Nara Women's University, Nara, Japan
[14] also at University of Tokyo, Tokyo, Japan
[15] Ramón y Cajal Fellow
[16] PPARC Postdoctoral Research Fellow
[17] on leave of absence at The National Science Foundation, Arlington, VA, USA
[18] now at University of London, Queen Mary College, London, UK
[19] present address: Tokyo Metropolitan University of Health Sciences, Tokyo 116-8551, Japan
[20] also at University of Hamburg, Alexander von Humboldt Fellow
[21] also at Łódź University, Poland
[22] supported by the Polish State Committee for Scientific Research, grant no. 2P03B 07222
[23] Łódź University, Poland
[24] Łódź University, Poland, supported by the KBN grant 2P03B12925
[25] supported by the KBN grant 2P03B12725
[26] on leave from MSU, partly supported by the Weizmann Institute via the U.S.-Israel BSF

Received: 8 April 2004 / Revised version: 10 May 2004 /
Published online: 18 June 2004 – © Springer-Verlag / Società Italiana di Fisica 2004

Abstract. The dependence of dijet production on the virtuality of the exchanged photon, Q^2, has been studied by measuring dijet cross sections in the range $0 \lesssim Q^2 < 2000\,\mathrm{GeV}^2$ with the ZEUS detector at HERA using an integrated luminosity of $38.6\,\mathrm{pb}^{-1}$. Dijet cross sections were measured for jets with transverse energy $E_T^{\mathrm{jet}} > 7.5$ and 6.5 GeV and pseudorapidities in the photon-proton centre-of-mass frame in the range $-3 < \eta^{\mathrm{jet}} < 0$. The variable x_γ^{obs}, a measure of the photon momentum entering the hard process, was used to enhance the sensitivity of the measurement to the photon structure. The Q^2 dependence of the ratio of low- to high-x_γ^{obs} events was measured. Next-to-leading-order QCD predictions were found to generally underestimate the low-x_γ^{obs} contribution relative to that at high x_γ^{obs}. Monte Carlo models based on leading-logarithmic parton-showers, using a partonic structure for the photon which falls smoothly with increasing Q^2, provide a qualitative description of the data.

1 Introduction

Interactions involving real or quasi-real photons ($Q^2 \approx 0$, where Q^2 is the virtuality of the photon) are well described by calculations that use a partonic structure for the photon [1,2]. However, in deep inelastic scattering (DIS), where Q^2 is large, the virtual photon is commonly treated as a point-like object and used as a probe of the partonic structure of nucleons [3–5]. In this paper, dijet production is investigated over a large range of incident photon virtualities, including photoproduction, DIS, and the transition region between them. Both the H1 [6,7] and ZEUS [8] collaborations have previously studied the transition between photoproduction and DIS by measuring inclusive jet and dijet cross sections in ep collisions.

[a] supported by the Natural Sciences and Engineering Research Council of Canada (NSERC)
[b] supported by the German Federal Ministry for Education and Research (BMBF), under contract numbers HZ1GUA 2, HZ1GUB 0, HZ1PDA 5, HZ1VFA 5
[c] supported by the MINERVA Gesellschaft für Forschung GmbH, the Israel Science Foundation, the U.S.-Israel Binational Science Foundation and the Benozyio Center for High Energy Physics
[d] supported by the German-Israeli Foundation and the Israel Science Foundation
[e] supported by the Italian National Institute for Nuclear Physics (INFN)
[f] supported by the Japanese Ministry of Education, Culture, Sports, Science and Technology (MEXT) and its grants for Scientific Research
[g] supported by the Korean Ministry of Education and Korea Science and Engineering Foundation
[h] supported by the Netherlands Foundation for Research on Matter (FOM)
[i] supported by the Polish State Committee for Scientific Research, grant no. 620/E-77/SPB/DESY/P-03/DZ 117/2003–2005
[j] partially supported by the German Federal Ministry for Education and Research (BMBF)
[k] supported by RF President grant N 1685.2003.2 for the leading scientific schools and by the Russian Ministry of Industry, Science and Technology through its grant for Scientific Research on High Energy Physics
[l] supported by the Spanish Ministry of Education and Science through funds provided by CICYT
[m] supported by the Particle Physics and Astronomy Research Council, UK
[n] supported by the US Department of Energy
[o] supported by the US National Science Foundation
[p] supported by the Polish Ministry of Scientific Research and Information Technology, grant no. 112/E-356/SPUB/DESY/P-03/DZ 116/2003–2005
[q] supported by the Polish State Committee for Scientific Research, grant no. 115/E-343/SPUB-M/DESY/P-03/DZ 121/2001–2002, 2 P03B 07022

Two processes contribute to the jet photoproduction cross section at leading order (LO) in quantum chromodynamics (QCD) [9–18]: direct, in which the photon couples as a point-like particle to quarks in the hard scatter; and resolved, in which the photon acts as a source of partons. Both processes can lead to two jets in the final state. The $x_\gamma^{\rm obs}$ variable, which is the fraction of the photon momentum participating in the production of the dijet system, is used to separate the two processes since resolved (direct) processes dominate at low (high) $x_\gamma^{\rm obs}$ values [19, 20].

In conventional fixed-order QCD calculations, only point-like photon interactions contribute to jet production in DIS. However, two scales play a role in the interaction: Q and the jet transverse energy, $E_T^{\rm jet}$. For high Q^2 ($Q^2 \gg (E_T^{\rm jet})^2$), QCD predicts that the photon will behave as a point-like object. For $Q^2 \ll (E_T^{\rm jet})^2$, the photon may have an effective partonic structure, even for relatively large values of Q^2, which is resolved at a scale related to the transverse energy of the jets. Therefore, resolved processes may contribute significantly to the jet cross section. The ratio of cross sections evaluated in different $x_\gamma^{\rm obs}$ ranges is particularly sensitive to the resolved component.

In this paper, the validity of the above approaches in photoproduction and DIS is studied by measuring dijet cross sections differential with respect to Q^2, $E_T^{\rm jet1}$ and η^F, where $E_T^{\rm jet1}$ is the E_T of the jet in the accepted rapidity range which has the highest transverse energy, and η^F is the pseudorapidity of the most forward jet. The ratio of low- to high-$x_\gamma^{\rm obs}$ components is measured as a function of Q^2 in different regions of $\overline{E}_T^2$, where $\overline{E}_T^2$ is the square of the average transverse energy of the two jets with highest transverse energy.

The data used in this analysis correspond to an integrated luminosity six times larger than that used in the previous ZEUS study [8]. Next-to-leading-order (NLO) QCD calculations [21–25] have been compared to measurements that span a large range of photon virtualities. The predictions of leading-logarithm parton-shower (PS) Monte Carlo (MC) models are compared to the data in the transition region between photoproduction and DIS, where current NLO calculations are not applicable.

2 Experimental set-up

The data were collected during the 1996 and 1997 running periods, when HERA operated with protons of energy $E_p = 820\,\text{GeV}$ and positrons of energy $E_e = 27.5\,\text{GeV}$, and correspond to an integrated luminosity of $38.6 \pm 0.6\,\text{pb}^{-1}$.

The ZEUS detector is described in detail elsewhere [26]. The most important components used in the current analysis were the central tracking detector (CTD), the uranium-scintillator calorimeter (CAL) and the beam pipe calorimeter (BPC).

Charged particles are tracked in the central tracking detector (CTD) [27–29], which operates in a magnetic field of 1.43 T provided by a thin superconducting solenoid. The CTD consists of 72 cylindrical drift chamber layers, organised in nine superlayers covering the polar-angle[1] region $15^\circ < \theta < 164^\circ$. The transverse-momentum resolution for full-length tracks is $\sigma(p_T)/p_T = 0.0058 p_T \oplus 0.0065 \oplus 0.0014/p_T$, with p_T in GeV.

The high-resolution uranium–scintillator calorimeter (CAL) [30–33] consists of three parts: the forward (FCAL), the barrel (BCAL) and the rear (RCAL) calorimeters. Each part is subdivided transversely into towers and longitudinally into one electromagnetic section (EMC) and either one (in RCAL) or two (in BCAL and FCAL) hadronic sections (HAC). The smallest subdivision of the calorimeter is called a cell. The CAL energy resolutions, as measured under test-beam conditions, are $\sigma(E)/E = 0.18/\sqrt{E}$ for electrons and $\sigma(E)/E = 0.35/\sqrt{E}$ for hadrons, with E in GeV.

The BPC [34] was installed 294 cm from the interaction point in the positron direction in order to tag scattered positrons at small angles with respect to the positron beam direction (15–34 mrad). It measured both the energy and impact position of the scattered positron at the BPC surface. The relative energy resolution of the BPC is $0.17/\sqrt{E}$ and the position resolution is 0.5 mm.

The luminosity was determined from the rate of the bremsstrahlung process $ep \to e\gamma p$, where the photon was measured with a lead-scintillator calorimeter [35–37] at $Z = -107\,\text{m}$.

3 Theoretical framework

In photoproduction, perturbative QCD (pQCD) calculations of dijet cross sections can be written as a convolution of the subprocess cross section with the parton distribution functions (PDFs) of the photon and proton:

$$d\sigma_{ep\to e\,\text{jet jet}} = \sum_{a,b} \int_0^1 dy f_{\gamma/e}(y,\mu_R^2) \times \int_0^1 dx_\gamma f_{a/\gamma}(x_\gamma,\mu_R^2,\mu_{F\gamma}^2) \times \int_0^1 dx_p f_{b/p}(x_p,\mu_{Fp}^2)\, d\hat{\sigma}_{ab\to\text{jet jet}}(\mu_R),$$

where y, x_γ and x_p are the longitudinal momentum fractions of the almost-real photon emitted by the positron, the parton a in the photon and the parton b in the proton, respectively. The function $f_{\gamma/e}$ is the flux of photons from the positron, and $f_{a/\gamma}$ ($f_{b/p}$) represents the PDF of parton a (b) in the photon (proton). The factorisation scale for the photon (proton) is denoted by $\mu_{F\gamma}$ (μ_{Fp}) and μ_R represents the renormalisation scale. The subprocess cross section, $d\hat{\sigma}_{ab\to\text{jet jet}}$, describes the short-distance structure

[1] The ZEUS coordinate system is a right-handed Cartesian system, with the Z axis pointing in the proton beam direction, referred to as the "forward direction", and the X axis pointing left towards the centre of HERA. The coordinate origin is at the nominal interaction point.

of the interaction. For direct processes in the above formula a is replaced by γ and $f_{a/\gamma}(x_\gamma, Q^2, \mu^2_{F_\gamma})$ is given by $\delta(1-x_\gamma)$.

In DIS, the photons are virtual (γ^*) and usually only direct processes are considered. Effective resolved terms appear only as higher-order corrections.

In the transition region between DIS and photoproduction, a virtual-photon structure [38–47] may be introduced. In general, the virtual-photon PDFs f_{a/γ^*} contain two terms,

$$f_{a/\gamma^*}(x_{\gamma^*}, Q^2, \mu^2_{F_{\gamma^*}}) = f^{\mathrm{non-pert}}_{a/\gamma^*}(x_{\gamma^*}, Q^2, \mu^2_{F_{\gamma^*}}) + f^{\mathrm{pert}}_{a/\gamma^*}(x_{\gamma^*}, Q^2, \mu^2_{F_{\gamma^*}}),$$

the first associated with the non-perturbative hadronic component ($f^{\mathrm{non-pert}}$), in which the photon fluctuates into an intermediate meson-like hadronic state, and the second f^{pert}, unique to the photon, which expresses the coupling of the photon to a high-virtuality $q\bar{q}$ pair, calculable in pQCD. Perturbative QCD predicts that the contribution to the dijet cross section from resolved processes should decrease relative to the contribution from direct processes as the virtuality of the photon increases towards μ_R. The non-perturbative component of the virtual-photon PDFs decreases as Q^{-4}, whereas the perturbative component decreases as $\ln(\mu_R^2/Q^2)$.

Two parameterisations of the virtual-photon PDFs, SaS [38] and GRS [47], are available. Both are extrapolations of the real-photon PDFs to the virtual-photon regime. They differ in the treatment of the non-perturbative component. In the case of the SaS sets, a fit to a coherent sum of the lowest-lying vector-meson states ρ, ω and ϕ has been performed, whereas, in the case of GRS, the non-perturbative part has been estimated using the PDFs of the pion.

4 Cross section definition

Dijet cross sections differential in Q^2, E_T^{jet1} and η^F were measured. The ratios of cross sections for low (< 0.75) to high (> 0.75) x_γ^{obs} are presented. The variable x_γ^{obs} is defined as

$$x_\gamma^{\mathrm{obs}} = \frac{\sum_{\mathrm{jets}}(E^{\mathrm{jet}} - p_Z^{\mathrm{jet}})}{\sum_{\mathrm{hadrons}}(E - p_Z)} \ ,$$

where E^{jet} and p_Z^{jet} are the energy and the longitudinal momentum of the jet. The upper sum runs over the two jets with highest transverse energy and the lower sum runs over all final state hadrons.

The cross sections were measured in the range $0 \lesssim Q^2 < 2000\,\mathrm{GeV}^2$ and $0.2 < y < 0.55$. Jets were reconstructed with the k_T cluster algorithm [48] applied in the photon-proton centre-of-mass frame, in the longitudinally invariant inclusive mode [49]. At least two jets were required within the pseudorapidity range $-3 < \eta^{\mathrm{jet}} < 0$, satisfying $E_T^{\mathrm{jet1}} > 7.5\,\mathrm{GeV}$ and $E_T^{\mathrm{jet2}} > 6.5\,\mathrm{GeV}$.

5 Data selection and jet search

A three-level trigger was used to select events online [26,50]. In the third-level trigger the events were required to have at least two jets with a transverse energy of $E_T^{\mathrm{jet}} > 4\,\mathrm{GeV}$ and a pseudorapidity of $\eta^{\mathrm{jet}} < 2.5$ in the laboratory frame.

The sample was separated offline into subsamples corresponding to three different Q^2 ranges:

- DIS sample: events were selected by requiring that the outgoing positron was measured in the CAL [51]. The energy of the scattered positron, $E_{e'}$, was required to be above 10 GeV, with $1.5 < Q^2 < 2000\ \mathrm{GeV}^2$;
- BPC sample: events at low Q^2 were selected by requiring that the scattered positron was measured in the BPC. These events were required to have $E_{e'} > 12.5\,\mathrm{GeV}$ and $0.1 < Q^2 < 0.55\ \mathrm{GeV}^2$;
- Photoproduction sample: events were selected by requiring that the scattered positron was not observed in the CAL, implying $Q^2 < 1\,\mathrm{GeV}^2$ with a median $Q^2 \sim 10^{-3}\,\mathrm{GeV}^2$. A small fraction of this sample (0.6 %) is also contained in the BPC sample.

For all three samples, hadronic kinematic variables and jets were reconstructed using a combination of track and CAL information which optimises the resolution [52]. The selected tracks and CAL clusters are referred to as Energy Flow Objects (EFOs).

The method reported in a previous publication [53] was used to correct the EFOs for energy losses in inactive material in front of the CAL. The jet-energy-scale uncertainty is within ±1% for $E_T^{\mathrm{jet}} > 7.5\,\mathrm{GeV}$ and increases to ±3% for lower E_T^{jet} values.

Additional cuts, similar to those used in an earlier analysis [8], were applied offline to all samples:

- a reconstructed event vertex consistent with the nominal interaction position was required, $|Z_{\mathrm{vtx}}| < 40\,\mathrm{cm}$;
- to suppress the background from events with a misidentified positron, the variable $y_e = 1 - \frac{E_{e'}}{2E_{e'}(1-\cos\theta_{e'})}$ was required to satisfy $y_e < 0.8$, where $\theta_{e'}$ is the polar angle of the scattered positron;
- for the DIS sample, a fiducial volume cut was applied to the positron position ($|X_e| > 14\,\mathrm{cm}$ or $|Y_e| > 9\,\mathrm{cm}$, where X_e and Y_e are the impact positions of the positron on the face of the CAL) in order to avoid the low-acceptance region adjacent to the rear beam pipe;
- for the BPC sample, the reconstructed impact position on the BPC surface was constrained to be within the fiducial-region of the BPC [34];
- for the photoproduction sample, events with a scattered-positron candidate in the CAL were rejected, as in a previous ZEUS analysis [54];
- all samples were required to satisfy $0.2 < y_{\mathrm{JB}} < 0.55$, where $y_{\mathrm{JB}} = \sum_i (E_i - E_{Zi})/2E_e$ [55] is an estimator of y. The sum runs over all EFOs. $E_{Zi} = E_i \cos\theta_i$, where E_i is the energy of EFO i with polar angle θ_i with respect to the measured Z-vertex of the event. The lower cut removes beam-gas events and the upper cut is imposed due to the restricted acceptance of the BPC detector.

Prior to jet finding, the EFOs were boosted to the photon-proton centre-of-mass frame. In the DIS and BPC samples the boost was calculated using the reconstructed momentum of the scattered positron. In the photoproduction sample $y_{\rm JB}$ was used in performing the boost.

The k_T cluster algorithm was applied to the boosted EFOs in the photon-proton centre-of-mass frame to reconstruct jets. At least two jets were required in each event within the pseudorapidity range $-3 < \eta^{\rm jet} < 0$ and were ordered according to decreasing $E_T^{\rm jet}$. They were further required to satisfy $E_T^{\rm jet1} > 7.5\,{\rm GeV}$ and $E_T^{\rm jet2} > 6.5\,{\rm GeV}$. After all cuts, the photoproduction/BPC/DIS sample contained 419911/2481/45100 dijet events. The BPC sample is a subset of the photoproduction sample.

6 Acceptance corrections

The programs HERWIG 5.9 [56] and PYTHIA 6.1 [57] were used to generate events for resolved and direct processes over the whole Q^2 range. Events were generated using GRV-LO [58] for the photon PDFs and MRSA [59] for the proton PDFs. To study the dependence of the acceptance corrections on the choice of photon and proton PDFs, the GRS-LO and CTEQ5M1 [60] parameterisations were used, respectively. In both generators, the partonic processes are simulated using LO matrix elements, with the inclusion of initial- and final-state parton showers. Hadronisation is performed using a cluster model [61] in the case of HERWIG and the Lund string model [62] in the case of PYTHIA. For the measurements presented in this paper, the HERWIG and PYTHIA programs were used to correct the data for acceptance. The corrections provided by HERWIG were used as default values and those given by PYTHIA were used to estimate the systematic uncertainties associated with the treatment of the parton shower and hadronisation.

All generated events were passed through the ZEUS detector and trigger simulation programs based on GEANT 3.13 [63]. They were reconstructed and analysed by the same program chain as the data. The jet search was performed using EFOs in the same way as for the data. The same jet algorithm was also applied to the final-state particles. The jets found in this way are referred to as hadronic jets.

The acceptance corrections take into account the efficiency of the trigger, the selection criteria and the purity and efficiency of the jet reconstruction. The differential dijet cross sections were obtained by applying bin-by-bin corrections to the measured distributions. The predictions of the generators HERWIG and PYTHIA for the uncorrected distributions were compared to the data for the above parameterisations of the photon and proton PDFs. The contributions from direct and resolved processes were added according to a fit to the uncorrected $x_\gamma^{\rm obs}$ distribution in the data. A good description of the $E_T^{\rm jet}$, $\eta^{\rm jet}$, Q^2 and y data distributions was given by both HERWIG and PYTHIA.

For the photoproduction sample the bin-by-bin correction factor was approximately 1.2. This increased to approximately 6 for the BPC sample due to the geometric acceptance of the BPC detector [34]. For $1.5 < Q^2 < 4.5$ GeV^2, the correction factor was approximately 3 due to the fiducial volume cut (see Sect. 5). For $Q^2 > 4.5$ GeV^2, the bin-by-bin correction factors differed from unity by less than 10%.

7 QCD calculations

7.1 NLO calculations

The NLO QCD calculations of jet production cross sections in DIS used in this analysis are based on the programs DISASTER++ [21] and DISENT [22]. In these programs, the photon is treated as a point-like probe. Contributions from hadron-like resolved processes are not included. They use the subtraction method [64] and the massless $\overline{\rm MS}$ renormalisation and factorisation schemes. Their predictions agree to within $\pm 3\%$. In Sect. 9 only the calculations using DISASTER++ are compared to the data because this program allows a wider parameter selection than DISENT. In the calculations, the number of flavours was set to five. The renormalisation and factorisation scales were set to $\mu^2 = \mu_R^2 = \mu_F^2 = Q^2 + (E_T^{\rm jet})^2$ or Q^2, and $\alpha_s(\mu_R)$ was calculated at two loops using $\Lambda^{(5)}_{\overline{\rm MS}} = 226\,{\rm MeV}$ corresponding to $\alpha_S(M_Z) = 0.118$. The CTEQ5M1 sets were used for the proton PDFs.

Many calculations of jet photoproduction at NLO exist [23–25,65–69], all of which agree to within (5–10)% [69, 70]. The calculations of Frixione and Ridolfi [23–25] uses the subtraction method. In this calculation the number of flavours was set to five and the factorisation and renormalisation scales to $\mu^2 = (E_T^{\rm jet})^2$. For the calculation of $\alpha_s(\mu_R)$, $\Lambda^{(5)}_{\overline{\rm MS}} = 226\,{\rm MeV}$ was used. For the proton PDFs, the CTEQ5M1 sets were used, and for the real photon PDFs the GRV and AFG [71] parameterisations were used.

Samples of events generated using the HERACLES 4.6.1 [72, 73] MC program with the DJANGOH 1.1 [74–76] interface to the hadronisation programs were used to estimate hadronisation corrections for the NLO QCD predictions calculated using DISENT and DISASTER++. The QCD cascade is simulated using the colour-dipole model [77–80] including the LO QCD diagrams as implemented in ARIADNE 4.08 [81] or with the MEPS model of LEPTO 6.5 [82]. Both ARIADNE and LEPTO use the Lund string model [62] for the hadronisation. For the photoproduction NLO prediction, the HERWIG and PYTHIA MCs were used to estimate the hadronisation corrections.

First-order QED radiative effects were also estimated using HERACLES and found to be 1% or less. Corrections for these effects have not been applied to the NLO calculations.

The predictions to be compared with the data were corrected for hadronisation effects using a bin-by-bin procedure according to $d\sigma = d\sigma^{\rm NLO} \cdot C_{\rm had}^{-1}$, where $d\sigma^{\rm NLO}$ is the cross section for partons in the final state of the NLO calculation. The hadronisation correction factor was defined as the ratio of the dijet cross sections before and after the hadronisation process, $C_{\rm had} = d\sigma_{\rm MC}^{\rm partons}/d\sigma_{\rm MC}^{\rm hadrons}$. The value of $C_{\rm had}$ was taken as the mean of the ratio obtained

using the predictions of two different generators (ARIADNE and LEPTO for DIS, and HERWIG and PYTHIA for photoproduction) and was found to lie between 1.1 (large Q^2) and 1.2 (small Q^2 and photoproduction).

7.2 Monte Carlo predictions

Predictions of HERWIG 6.4 [83] using CTEQ5L for the proton PDFs and SaS2D for the photon PDFs were generated using parameters tuned [84] to many previous HERA and LEP measurements. In the SaS2D parameterisation the structure of the virtual photon is suppressed with increasing Q^2. Predictions were also generated with this suppression switched off.

8 Systematic uncertainties

8.1 Experimental uncertainties

A detailed study of the sources contributing to the systematic uncertainties of the measurements was performed. This study includes (a typical contribution to the uncertainty in the cross section for each item is indicated in parentheses):

- using the PYTHIA generator to evaluate the acceptance corrections to the observed dijet distributions (+6%);
- using different parameterisations of the photon (GRV-LO and GRS) and proton (MRSA and CTEQ5M1) PDFs for the generation of the HERWIG MC samples (±2%);
- varying the $E_T^{\rm jet}$ cut by the resolution (±8%);
- varying the other selection cuts by their respective resolution (< ±2%)
- adding the contributions from direct and resolved processes according to the default cross sections as predicted by HERWIG (−3%).

All the above systematic uncertainties were added in quadrature. The effect of the uncertainty in the absolute energy scale of the jets on the dijet cross sections was approximately ±9% at low Q^2, decreasing to ±6% at high Q^2. This uncertainty is highly correlated and is shown separately in the figures. In addition, there is an overall normalisation uncertainty from the luminosity determination of 1.6%, which is not shown in the figures.

8.2 Theoretical uncertainties

The NLO QCD predictions for the dijet cross sections are affected by the following theoretical uncertainties (typical values for the uncertainties are quoted):

- uncertainties due to terms beyond NLO, estimated by varying μ by factors 2 and 0.5 (20% at low Q^2 and 7% at high Q^2, in the case of $\mu^2 = Q^2 + (E_T^{\rm jet})^2$);
- uncertainties in the hadronisation corrections, estimated as half the spread between $C_{\rm had}$ values obtained using the HERWIG, PYTHIA, LEPTO and ARIADNE models (2–3%);
- uncertainties on the calculations due to α_S and the proton PDFs, estimated by using the MRST sets of parameterisations (5%). These uncertainties were cross-checked using an alternative method [85], which uses the covariance matrix of the fitted PDF parameters and derivatives as a function of x.

The above theoretical uncertainties were added in quadrature to give the total uncertainty on the predictions.

9 Results

9.1 Single-differential dijet cross sections

Figure 1 shows the differential dijet cross section, $d\sigma/dQ^2$, for $E_T^{\rm jet1} > 7.5\,{\rm GeV}$, $E_T^{\rm jet2} > 6.5\,{\rm GeV}$, $-3 < \eta^{\rm jet} < 0$, $0.2 <$

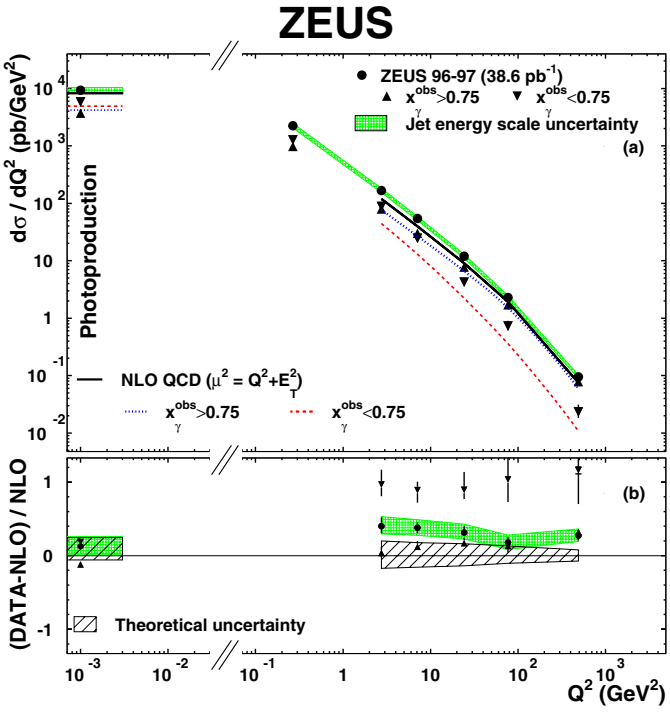

Fig. 1. a Measured dijet cross sections $d\sigma/dQ^2$ for $x_\gamma^{\rm obs} \geq 0.75$ (upwards triangles) $d\sigma/dQ^2$ for $x_\gamma^{\rm obs} < 0.75$ (downwards triangles) and $d\sigma/dQ^2$ for the entire $x_\gamma^{\rm obs}$ region (black dots). The inner vertical bars represent the statistical uncertainties of the data, and the outer bars show the statistical and systematic uncertainties added in quadrature, except for that associated with the uncertainty in the absolute energy scale of the jets (shaded band). The NLO QCD calculations of DISASTER++ ($\mu^2 = Q^2 + (E_T^{\rm jet})^2$) and of Frixione and Ridolfi ($\mu^2 = (E_T^{\rm jet})^2$) for the photoproduction region are shown for each of the cross sections. **b** Relative difference of the measured dijet cross section $d\sigma/dQ^2$ to the DISASTER++ ($\mu^2 = Q^2 + (E_T^{\rm jet})^2$) and of Frixione and Ridolfi ($\mu^2 = (E_T^{\rm jet})^2$) calculations. The hatched band shows the theoretical uncertainty of the calculations (see text)

Table 1. Measured dijet cross-sections $d\sigma/dQ^2$. The statistical, systematic and jet energy scale, $\Delta_{\rm ES}$, uncertainties are shown separately

Q^2 bin (GeV^2)	$d\sigma/dQ^2$	$\Delta_{\rm stat}$	$\Delta_{\rm syst}$	$\Delta_{\rm ES}$
		($\mathrm{pb/GeV}^2$)		
0, 1	9280	± 113	$^{+102}_{-69.3}$	$^{+917}_{-1100}$
0.1, 0.55	2250	± 45.2	$^{+215}_{-210}$	$^{+194}_{-227}$
1.5, 4.5	167	± 2.22	$^{+14.1}_{-11.9}$	$^{+12.5}_{-15.2}$
4.5, 10.5	54.5	± 0.54	$^{+3.05}_{-2.76}$	$^{+3.94}_{-4.48}$
10.5, 49	11.9	± 0.093	$^{+0.79}_{-0.32}$	$^{+0.81}_{-1.01}$
49, 120	2.27	± 0.027	$^{+0.14}_{-0.13}$	$^{+0.17}_{-0.2}$
120, 2000	0.095	± 0.0011	$^{+0.0019}_{-0.0048}$	$^{+0.0059}_{-0.0068}$

Table 2. Measured dijet cross-sections $d\sigma/dQ^2$ for $x_\gamma^{\rm obs} < 0.75$. The statistical and systematic uncertainties are shown separately

Q^2 bin (GeV^2)	$d\sigma/dQ^2$	$\Delta_{\rm stat}$	$\Delta_{\rm syst}$
		($\mathrm{pb/GeV}^2$)	
0, 1	5710	± 96.4	$^{+63}_{-41.7}$
0.1, 0.55	1270	± 32.3	$^{+197}_{-141}$
1.5, 4.5	87.8	± 1.54	$^{+8.89}_{-7.01}$
4.5, 10.5	24.5	± 0.35	$^{+1.39}_{-2.22}$
10.5, 49	4.21	± 0.051	$^{+0.53}_{-0.27}$
49, 120	0.72	± 0.015	$^{+0.17}_{-0.1}$
120, 2000	0.022	± 0.00052	$^{+0.0081}_{-0.0049}$

Table 3. Measured dijet cross-sections $d\sigma/dQ^2$ for $x_\gamma^{\rm obs} > 0.75$. The statistical and systematic uncertainties are shown separately

Q^2 bin (GeV^2)	$d\sigma/dQ^2$	$\Delta_{\rm stat}$	$\Delta_{\rm syst}$
		($\mathrm{pb/GeV}^2$)	
0, 1	3620	± 65.8	$^{+39.2}_{-31.3}$
0.1, 0.55	980	± 31.9	$^{+32.8}_{-87.2}$
1.5, 4.5	79.5	± 1.61	$^{+6.01}_{-4.06}$
4.5, 10.5	30	± 0.42	$^{+2.03}_{-0.63}$
10.5, 49	7.74	± 0.08	$^{+0.5}_{-0.27}$
49, 120	1.63	± 0.024	$^{+0.15}_{-0.13}$
120, 2000	0.077	± 0.0011	$^{+0.0013}_{-0.0057}$

$y < 0.55$ and $0.1 < Q^2 < 2000\,\mathrm{GeV}^2$ together with the photoproduction measurement. The cross section split in the direct-enhanced region ($x_\gamma^{\rm obs} \geq 0.75$) and the resolved-enhanced region ($x_\gamma^{\rm obs} < 0.75$) is also shown. All the cross sections are given in the Tables 1, 2, and 3.

The measurements cover a wide range in Q^2, including the transition region from photoproduction to DIS. The measured cross sections fall by about five orders of magnitude over this Q^2 range. The cross section for $x_\gamma^{\rm obs} < 0.75$ falls more rapidly than that for $x_\gamma^{\rm obs} > 0.75$. Even though the dijet cross section is dominated by interactions with $x_\gamma^{\rm obs} > 0.75$ for $Q^2 \gtrsim 10\,\mathrm{GeV}^2$, there is a

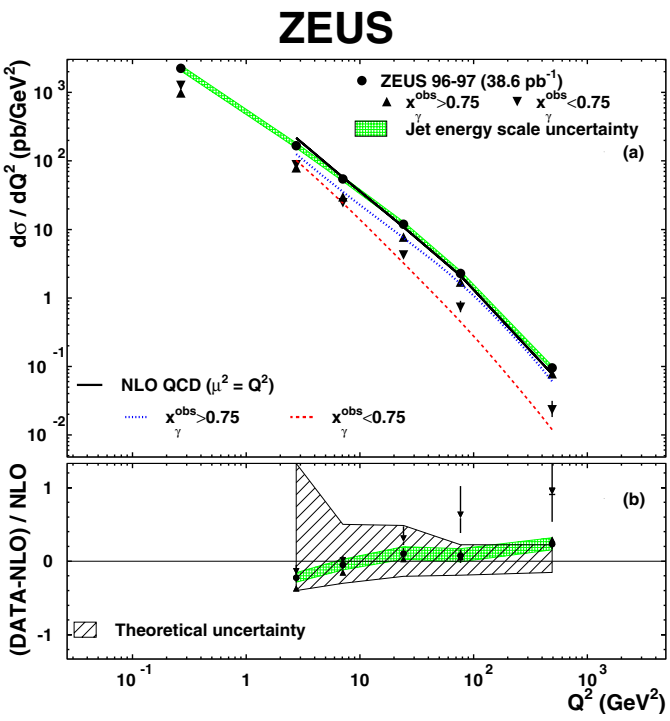

Fig. 2. a Measured dijet cross sections $d\sigma/dQ^2$ for $x_\gamma^{\rm obs} \geq 0.75$ (upwards triangles) $d\sigma/dQ^2$ for $x_\gamma^{\rm obs} < 0.75$ (downwards triangles) and $d\sigma/dQ^2$ for the entire $x_\gamma^{\rm obs}$ region (black dots). The inner vertical bars represent the statistical uncertainties of the data, and the outer bars show the statistical and systematic uncertainties added in quadrature, except for that associated with the uncertainty in the absolute energy scale of the jets (shaded band). The NLO QCD calculations of DISASTER++ with $\mu^2 = Q^2$ are shown for each of the cross sections. **b** Relative difference of the measured dijet cross section $d\sigma/dQ^2$ to the DISASTER++calculation with $\mu^2 = Q^2$. The hatched band shows the theoretical uncertainty of the calculation

contribution of approximately 24% from low-$x_\gamma^{\rm obs}$ events with $Q^2 \simeq 500\,\mathrm{GeV}^2$.

The NLO QCD calculations are compared to the measured $d\sigma/dQ^2$ in Figs. 1 and 2. The prediction[2] with $\mu^2 = Q^2 + (E_T^{\rm jet})^2$, shown in Fig. 1, describes the shape of the measured total dijet cross section but underestimates its magnitude by approximately 30%. The renormalisation scale uncertainty was evaluated also for the low- and high-$x_\gamma^{\rm obs}$ cross sections. For the high-$x_\gamma^{\rm obs}$ cross section this uncertainty was similar to that on the total cross section. In the case of the low-$x_\gamma^{\rm obs}$ cross section, the uncertainty was almost constant at around $\pm 30\%$. Taking these uncertainties into account, the measured cross section for $x_\gamma^{\rm obs} > 0.75$ is reasonably well described by the calculation shown in Fig. 1a for all Q^2. However, the prediction dramatically underestimates the measured cross section for $x_\gamma^{\rm obs} < 0.75$.

The prediction with $\mu^2 = Q^2$ is shown in Fig. 2. It has a much larger renormalisation-scale uncertainty than

[2] The two lowest Q^2 bins are outside the range of applicability of the DISASTER++ program.

the prediction using $\mu^2 = Q^2 + (E_T^{\rm jet})^2$, and within this uncertainty it is consistent with the data.

A possible explanation of the disagreement, and for the large uncertainties in the prediction at low-$x_\gamma^{\rm obs}$ values, is that effects arising from the structure of the photon are expected in this region, whereas the contribution predicted by DISASTER++ comes only from large-angle particle-emission diagrams included in the NLO corrections to the dijet cross section.

In photoproduction, the low-$x_\gamma^{\rm obs}$ component of the data becomes dominant. The photoproduction measurement is well described by the photoproduction NLO prediction, using the GRV photon PDF.

9.2 Double-differential dijet cross sections

The dijet cross section, $d^2\sigma/dQ^2dE_T^{\rm jet1}$, as a function of $E_T^{\rm jet1}$ in different Q^2 ranges is shown in Fig. 3 and given in the Tables 4 and 5. The measurements extend up to transverse energies of approximately 40 GeV. The $E_T^{\rm jet1}$ distribution falls less steeply as Q^2 increases. Figure 3 also shows the NLO QCD predictions. The NLO calculation for photoproduction using GRV for the photon PDFs gives a good description of the $E_T^{\rm jet1}$ cross section. At higher Q^2, the calculation using $\mu^2 = Q^2 + (E_T^{\rm jet})^2$ is in agreement with the data for the lowest and highest jet transverse energies, but lies below the data for intermediate $E_T^{\rm jet1}$ values. The

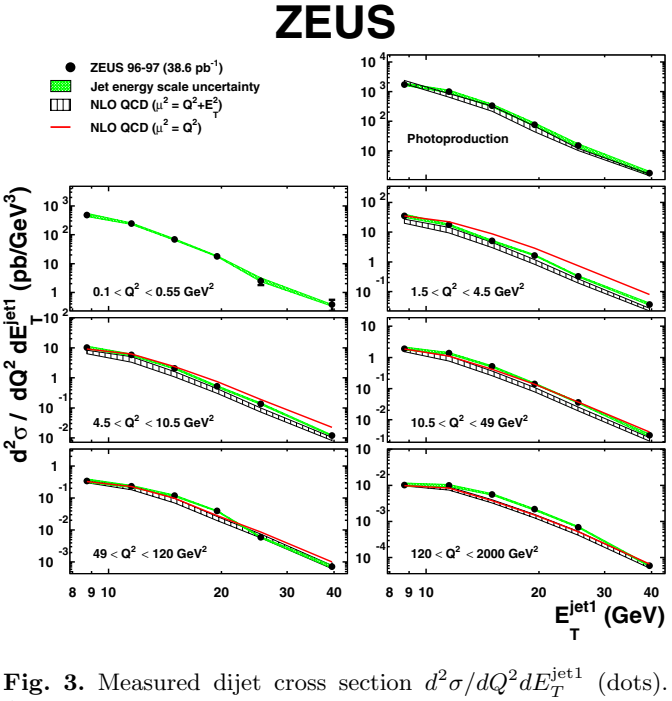

Fig. 3. Measured dijet cross section $d^2\sigma/dQ^2dE_T^{\rm jet1}$ (dots). Also shown are the NLO QCD calculations of DISASTER++ with $\mu^2 = Q^2 + (E_T^{\rm jet})^2$ and $\mu^2 = Q^2$, and those of Frixione and Ridolfi for the photoproduction region. The scale uncertainty for the NLO calculation with $\mu^2 = Q^2$ is not shown. Other details are as in Fig. 1

Table 4. Measured dijet cross-section $d^2\sigma/dQ^2dE_T^{\rm jet1}$

$E_T^{\rm jet1}$ bin (GeV)	$d^2\sigma/dE_T^{\rm jet1}dQ^2$ (pb/GeV^3)	$\Delta_{\rm stat}$	$\Delta_{\rm syst}$	$\Delta_{\rm ES}$
$0 < Q^2 < 1$ GeV^2				
7.5, 10	1740	±34.8	$^{+20.9}_{-84.3}$	$^{+146}_{-189}$
10, 13	1010	±20.4	$^{+11.3}_{-24.8}$	$^{+90}_{-118}$
13, 17	337	±8.5	$^{+21.5}_{-8.51}$	$^{+35.7}_{-39.9}$
17, 22	76.4	±3.22	$^{+3.9}_{-3.14}$	$^{+9.45}_{-9.6}$
22, 29	15	±1.25	$^{+0.1}_{-0.085}$	$^{+1.96}_{-2.03}$
29, 50	1.75	±0.092	$^{+0.37}_{-0.16}$	$^{+0.22}_{-0.23}$
$0.1 < Q^2 < 0.55$ GeV^2				
7.5, 10	484	±22.6	$^{+24.3}_{-75.5}$	$^{+53.6}_{-70.3}$
10, 13	243	±12.1	$^{+6.81}_{-14.7}$	$^{+16.8}_{-15}$
13, 17	68.7	±4.91	$^{+4.92}_{-1.38}$	$^{+4.22}_{-3.53}$
17, 22	17.9	±2.19	$^{+1.33}_{-1.76}$	$^{+0.48}_{-0.94}$
22, 29	2.49	±0.67	$^{+0.39}_{-0.29}$	$^{+0.13}_{-0.69}$
29, 50	0.38	±0.17	$^{+0.071}_{-0.083}$	$^{+0.048}_{-0}$
$1.5 < Q^2 < 4.5$ GeV^2				
7.5, 10	35.2	±0.72	$^{+2.46}_{-1.31}$	$^{+3.44}_{-4.71}$
10, 13	17.6	±0.41	$^{+0.96}_{-1}$	$^{+0.96}_{-1.12}$
13, 17	5.09	±0.16	$^{+0.52}_{-0.044}$	$^{+0.36}_{-0.26}$
17, 22	1.64	±0.091	$^{+0.032}_{-0.13}$	$^{+0.057}_{-0.086}$
22, 29	0.32	±0.033	$^{+0.0087}_{-0.035}$	$^{+0.015}_{-0.01}$
29, 50	0.037	±0.0063	$^{+0.0023}_{-0.0049}$	$^{+0.0024}_{-0.0035}$
$4.5 < Q^2 < 10.5$ GeV^2				
7.5, 10	10.2	±0.16	$^{+0.23}_{-1.32}$	$^{+1}_{-1.21}$
10, 13	5.86	±0.1	$^{+0.25}_{-0.16}$	$^{+0.34}_{-0.37}$
13, 17	2.08	±0.048	$^{+0.043}_{-0.061}$	$^{+0.11}_{-0.12}$
17, 22	0.52	±0.02	$^{+0.0084}_{-0.033}$	$^{+0.034}_{-0.019}$
22, 29	0.13	±0.0097	$^{+0.0071}_{-0.0078}$	$^{+0.0053}_{-0.011}$
29, 50	0.011	±0.0015	$^{+0.002}_{-0.00084}$	$^{+0.00039}_{-0.00059}$

prediction with $\mu^2 = Q^2$ again agrees with the data, within the large theoretical uncertainties (not shown).

The differential cross-section $d^2\sigma/dQ^2d\eta^F$ as a function of η^F is shown in Fig. 4 for different ranges of Q^2 and given in the Tables 6 and 7. The cross section as a function of η^F is more sensitive to the resolved photon component in the forward direction[3]. In all Q^2 regions, the measured cross section increases with η^F in the region $-2.5 < \eta^F < -1.5$. For $\eta^F > -1.5$, the cross section decreases as η^F increases for $Q^2 \gtrsim 10\,{\rm GeV}^2$, whereas in photoproduction and at low Q^2 the cross section increases. The NLO prediction for photoproduction describes the measured cross section. At low Q^2 the NLO prediction using $\mu^2 = Q^2 + (E_T^{\rm jet})^2$ underestimates the measured cross section in the forward direc-

[3] Since η here is defined in the hadronic centre-of-mass frame, the forward region in the laboratory frame corresponds to $\eta > -1$.

Table 5. Measured dijet cross-section $d^2\sigma/dQ^2dE_T^{\mathrm{jet1}}$

E_T^{jet1} bin (GeV)	$d^2\sigma/dE_T^{\mathrm{jet1}}dQ^2$	Δ_{stat}	Δ_{syst}	Δ_{ES}
		(pb/GeV^3)		
$10.5 < Q^2 < 49\,\mathrm{GeV}^2$				
7.5, 10	1.9	±0.024	$^{+0.15}_{-0.059}$	$^{+0.17}_{-0.25}$
10, 13	1.36	±0.018	$^{+0.057}_{-0.041}$	$^{+0.091}_{-0.082}$
13, 17	0.51	±0.0091	$^{+0.024}_{-0.013}$	$^{+0.028}_{-0.025}$
17, 22	0.14	±0.0041	$^{+0.0029}_{-0.007}$	$^{+0.0031}_{-0.0086}$
22, 29	0.036	±0.0018	$^{+0.0014}_{-0.0021}$	$^{+0.0017}_{-0.0012}$
29, 50	0.0031	±0.00031	$^{+0.00018}_{-0.00011}$	$^{+0.00028}_{-0.00034}$
$49 < Q^2 < 120\,\mathrm{GeV}^2$				
7.5, 10	0.34	±0.0071	$^{+0.025}_{-0.024}$	$^{+0.038}_{-0.053}$
10, 13	0.23	±0.0049	$^{+0.014}_{-0.011}$	$^{+0.018}_{-0.016}$
13, 17	0.11	±0.0031	$^{+0.0016}_{-0.0071}$	$^{+0.0058}_{-0.0047}$
17, 22	0.039	±0.0016	$^{+0.00087}_{-0.001}$	$^{+0.0011}_{-0.0014}$
22, 29	0.0059	±0.00047	$^{+0.001}_{-0.00023}$	$^{+0.00031}_{-0.00018}$
29, 50	0.00072	$\pm8.5\times10^{-5}$	$^{+0.00023}_{-3\times10^{-5}}$	$^{+8.3\times10^{-5}}_{-5.2\times10^{-5}}$
$120 < Q^2 < 2000\,\mathrm{GeV}^2$				
7.5, 10	0.01	±0.00025	$^{+0.00041}_{-0.00098}$	$^{+0.001}_{-0.0014}$
10, 13	0.0099	±0.00021	$^{+0.00043}_{-0.00076}$	$^{+0.00059}_{-0.0006}$
13, 17	0.0056	±0.00014	$^{+0.00011}_{-0.00023}$	$^{+0.00022}_{-0.00025}$
17, 22	0.0021	$\pm7.7\times10^{-5}$	$^{+6.7\times10^{-5}}_{-0.00011}$	$^{+0.00014}_{-6.4\times10^{-5}}$
22, 29	0.00069	$\pm3.6\times10^{-5}$	$^{+7.1\times10^{-5}}_{-3.9\times10^{-5}}$	$^{+1.8\times10^{-5}}_{-3.3\times10^{-5}}$
29, 50	6×10^{-5}	$\pm5.2\times10^{-6}$	$^{+5\times10^{-6}}_{-4.2\times10^{-6}}$	$^{+3.4\times10^{-6}}_{-2\times10^{-6}}$

Table 6. Measured dijet cross-section $d^2\sigma/dQ^2d\eta^F$

η^F bin	$d^2\sigma/d\eta^F dQ^2$	Δ_{stat}	Δ_{syst}	Δ_{ES}
	(pb/GeV^2)			
$0 < Q^2 < 1\,\mathrm{GeV}^2$				
-3, -1.8	771	±27.5	$^{+39.1}_{-38.3}$	$^{+92.8}_{-119}$
-1.8, -1.4	3790	±108	$^{+130}_{-49.8}$	$^{+305}_{-335}$
-1.4, -0.8	4510	±96.9	$^{+162}_{-55.9}$	$^{+399}_{-571}$
-0.8, 0	5300	±99.3	$^{+66.6}_{-229}$	$^{+494}_{-606}$
$0.1 < Q^2 < 0.55\,\mathrm{GeV}^2$				
-3, -1.8	229	±18.1	$^{+3.41}_{-28.6}$	$^{+35.3}_{-21.3}$
-1.8, -1.4	939	±64.2	$^{+77.3}_{-67.3}$	$^{+60.9}_{-98.9}$
-1.4, -0.8	1070	±55	$^{+132}_{-81.6}$	$^{+82.2}_{-102}$
-0.8, 0	1240	±58.7	$^{+165}_{-155}$	$^{+101}_{-126}$
$1.5 < Q^2 < 4.5\,\mathrm{GeV}^2$				
-3, -1.8	15.3	±0.62	$^{+1.62}_{-2.08}$	$^{+1.68}_{-2.05}$
-1.8, -1.4	75.8	±2.47	$^{+4.11}_{-8.29}$	$^{+5.58}_{-5.4}$
-1.4, -0.8	81.5	±1.96	$^{+10}_{-1.15}$	$^{+5.05}_{-7.21}$
-0.8, 0	87.1	±1.78	$^{+7.4}_{-8.2}$	$^{+6.37}_{-7.57}$
$4.5 < Q^2 < 10.5\,\mathrm{GeV}^2$				
-3, -1.8	6.67	±0.19	$^{+0.37}_{-0.62}$	$^{+0.78}_{-0.85}$
-1.8, -1.4	26	±0.61	$^{+3.17}_{-0.21}$	$^{+1.84}_{-2.06}$
-1.4, -0.8	26.8	±0.47	$^{+0.27}_{-2.12}$	$^{+1.63}_{-1.81}$
-0.8, 0	24.9	±0.41	$^{+2.16}_{-1.58}$	$^{+1.62}_{-1.97}$

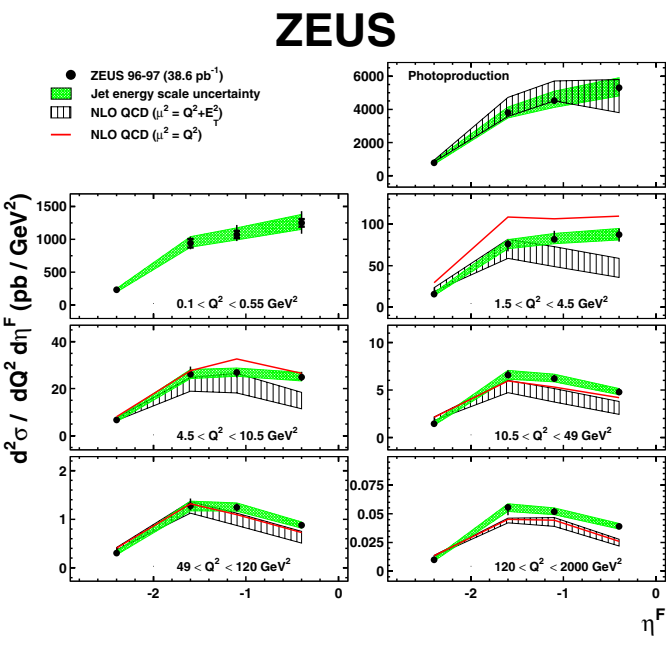

Fig. 4. Measured dijet cross section $d\sigma/dQ^2d\eta^F$ (black dots). The NLO QCD calculations of DISASTER++ with $\mu^2 = Q^2 + (E_T^{\mathrm{jet}})^2$ and $\mu^2 = Q^2$ as well as Frixione and Ridolfi for the photoproduction region are also shown. The scale uncertainty for the NLO calculation with $\mu^2 = Q^2$ is not shown. Other details are as in Fig. 1

Table 7. Measured dijet cross-section $d^2\sigma/dQ^2d\eta^F$

η^F bin	$d^2\sigma/d\eta^F dQ^2$	Δ_{stat}	Δ_{syst}	Δ_{ES}
	(pb/GeV^2)			
$10.5 < Q^2 < 49\,\mathrm{GeV}^2$				
-3, -1.8	1.45	±0.031	$^{+0.17}_{-0.036}$	$^{+0.15}_{-0.2}$
-1.8, -1.4	6.57	±0.11	$^{+0.48}_{-0.25}$	$^{+0.44}_{-0.47}$
-1.4, -0.8	6.21	±0.084	$^{+0.37}_{-0.16}$	$^{+0.36}_{-0.45}$
-0.8, 0	4.78	±0.064	$^{+0.4}_{-0.22}$	$^{+0.28}_{-0.37}$
$49 < Q^2 < 120\,\mathrm{GeV}^2$				
-3, -1.8	0.3	±0.01	$^{+0.032}_{-0.042}$	$^{+0.036}_{-0.045}$
-1.8, -1.4	1.27	±0.034	$^{+0.14}_{-0.08}$	$^{+0.098}_{-0.1}$
-1.4, -0.8	1.24	±0.026	$^{+0.074}_{-0.08}$	$^{+0.076}_{-0.09}$
-0.8, 0	0.87	±0.018	$^{+0.065}_{-0.056}$	$^{+0.059}_{-0.065}$
$120 < Q^2 < 2000\,\mathrm{GeV}^2$				
-3, -1.8	0.0097	±0.00035	$^{+9.2\times10^{-5}}_{-0.0011}$	$^{+0.00093}_{-0.0014}$
-1.8, -1.4	0.055	±0.0015	$^{+0.0011}_{-0.0067}$	$^{+0.0035}_{-0.0032}$
-1.4, -0.8	0.051	±0.001	$^{+0.003}_{-0.0012}$	$^{+0.0027}_{-0.0032}$
-0.8, 0	0.039	±0.00082	$^{+0.002}_{-0.0019}$	$^{+0.0022}_{-0.0024}$

tion. The prediction with $\mu^2 = Q^2$ again agrees reasonably well with the data within large theoretical uncertainties (not shown).

The differences between the data and NLO calculations may be due to the persistence of a resolved component at $Q^2 > 1\,\mathrm{GeV}^2$. To study this in more detail, the ratio of

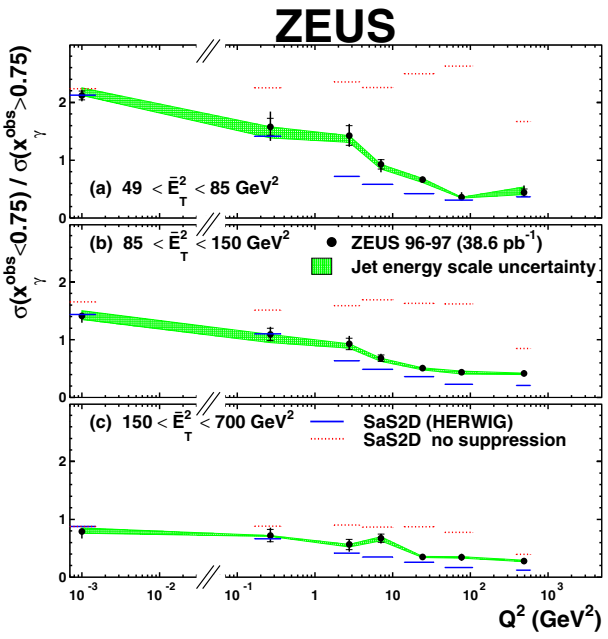

Fig. 5. Measured ratio $R = \sigma(x_\gamma^{\rm obs} < 0.75)/\sigma(x_\gamma^{\rm obs} > 0.75)$ as a function of Q^2 in different regions of $\overline{E}_T^2$ (black dots). The LO+PS calculations of HERWIG using the SaS2D photon PDFs are also shown. Other details are as in the caption to Fig. 1

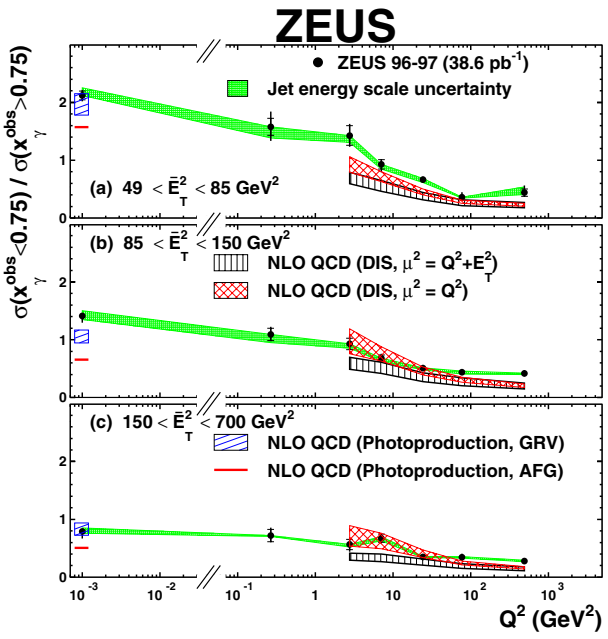

Fig. 6. Measured ratio $R = \sigma(x_\gamma^{\rm obs} < 0.75)/\sigma(x_\gamma^{\rm obs} > 0.75)$ as a function of Q^2 in different regions of $\overline{E}_T^2$ (black dots). The NLO QCD calculations of DISASTER++ with $\mu^2 = Q^2+(E_T^{\rm jet})^2$ and $\mu^2 = Q^2$ as well as the Frixione and Ridolfi predictions for the photoproduction region are also shown. The hatched bands represent the theoretical uncertainties. Other details areas in the caption to Fig. 1.

dijet cross sections for high and low $x_\gamma^{\rm obs}$ values is presented in the next subsection.

9.3 Ratios of dijet cross sections

The Q^2 dependence of the direct- and resolved-enhanced components of the dijet cross section has been studied in more detail using the ratio

$$R = \frac{\sigma(x_\gamma^{\rm obs} < 0.75)}{\sigma(x_\gamma^{\rm obs} > 0.75)} \, .$$

A number of experimental and theoretical uncertainties cancel in this ratio, so that the presence of a resolved contribution can be investigated at higher precision than in the individual cross sections.

Figures 5 and 6 show the ratio R as a function of Q^2 in three different regions of $\overline{E}_T^2$. The Q^2 dependence of the data is stronger at low $\overline{E}_T^2$ than at higher $\overline{E}_T^2$, showing that the low-$x_\gamma^{\rm obs}$ component is suppressed at low Q^2 as $\overline{E}_T^2$ increases, and at low $\overline{E}_T^2$ as Q^2 increases. The ratio is also given in Table 8.

Predictions of the HERWIG MC program using the SaS2D parameterisation of the photon PDFs are compared to the data in Fig. 5. The SaS2D parameterisation contains the suppression of the virtual photon structure with increasing Q^2. The predictions fall with increasing Q^2 and qualitatively reproduce the data. However, the predictions using SaS2D with the suppression of the virtual photon structure switched off are relatively constant with Q^2.

The NLO calculations are compared to the data in Fig. 6. The photoproduction calculations using GRV are in reasonable agreement with the data, whereas those using AFG are below the data. In the DIS region, the predictions lie below the data at low $\overline{E}_T^2$. However, some suppression in the ratio as a function of Q^2 is observed.

10 Summary and conclusions

Dijet differential cross sections have been measured in the range $0 \lesssim Q^2 < 2000\,{\rm GeV}^2$ with $0.2 < y < 0.55$, $-3 < \eta^{\rm jet} < 0$ and $E_T^{\rm jet1,jet2} > 7.5$ and $6.5\,{\rm GeV}$, as a function of Q^2, $E_T^{\rm jet1}$ and η^F in the photon-proton centre-of-mass frame. These precise measurements, spanning a large range of photon virtualities, including photoproduction, DIS, and the transition region between them, are qualitatively described by leading-logarithmic parton-shower MC models which introduce virtual photon structure, suppressed with increasing Q^2. These data may constrain such parton densities significantly if used in future fits.

The currently available next-to-leading-order QCD calculations have large uncertainties at low Q^2, where the presence of a resolved-photon contribution may be expected. Improved higher-order or resummed calculations are needed. In DIS, the NLO QCD predictions generally underestimate the cross section at low-$x_\gamma^{\rm obs}$ relative to that at high $x_\gamma^{\rm obs}$.

Table 8. Measured ratio $R = \sigma(x_\gamma^{\rm obs} < 0.75)/\sigma(x_\gamma^{\rm obs} > 0.75)$ as a function of Q^2 in different regions of $\overline{E}_T^2$

Q^2 bin	R	$\Delta_{\rm stat}$	$\Delta_{\rm syst}$	$\Delta_{\rm ES}$
$49 < \overline{E}_T^2 < 85\,{\rm GeV}^2$				
0, 1	2.12	±0.075	$^{+0.057}_{-0.066}$	$^{+0.0026}_{-0.12}$
0.1, 0.55	1.57	±0.14	$^{+0.22}_{-0.19}$	$^{+0.19}_{-0}$
1.5, 4.5	1.42	±0.16	$^{+0.1}_{-0.096}$	$^{+0.11}_{-0}$
4.5, 10.5	0.92	±0.08	$^{+0.035}_{-0.1}$	$^{+0.078}_{-0}$
10.5, 49	0.66	±0.039	$^{+0.029}_{-0.034}$	$^{+0.049}_{-0.021}$
49, 120	0.35	±0.037	$^{+0.079}_{-0.018}$	$^{+0.014}_{-0.0021}$
120, 2000	0.44	±0.063	$^{+0.1}_{-0.011}$	$^{+0.035}_{-0.1}$
$85 < \overline{E}_T^2 < 150\,{\rm GeV}^2$				
0, 1	1.41	±0.048	$^{+0.016}_{-0.1}$	$^{+0.065}_{-0.086}$
0.1, 0.55	1.09	±0.1	$^{+0.079}_{-0.044}$	$^{+0.13}_{-0}$
1.5, 4.5	0.92	±0.1	$^{+0.095}_{-0.032}$	$^{+0.073}_{-0}$
4.5, 10.5	0.68	±0.057	$^{+0.052}_{-0.026}$	$^{+0.053}_{-0}$
10.5, 49	0.51	±0.027	$^{+0.044}_{-0.023}$	$^{+0.033}_{-0.0036}$
49, 120	0.43	±0.038	$^{+0.029}_{-0.015}$	$^{+0.029}_{-0.019}$
120, 2000	0.41	±0.048	$^{+0.033}_{-0.0084}$	$^{+0.018}_{-0.0062}$
$150 < \overline{E}_T^2 < 700\,{\rm GeV}^2$				
0, 1	0.78	±0.032	$^{+0.0022}_{-0.11}$	$^{+0.028}_{-0.06}$
0.1, 0.55	0.72	±0.1	$^{+0.086}_{-0.049}$	$^{+0.018}_{-0}$
1.5, 4.5	0.56	±0.088	$^{+0.015}_{-0.088}$	$^{+0.042}_{-0}$
4.5, 10.5	0.67	±0.07	$^{+0.03}_{-0.059}$	$^{+0.043}_{-0.028}$
10.5, 49	0.34	±0.026	$^{+0.015}_{-0.0057}$	$^{+0.0092}_{-0.0098}$
49, 120	0.34	±0.039	$^{+0.046}_{-0.049}$	$^{+0.016}_{-0.0068}$
120, 2000	0.28	±0.046	$^{+0.019}_{-0.0052}$	$^{+0.014}_{-0.011}$

Acknowledgements. The design, construction and installation of the ZEUS detector have been made possible by the ingenuity and dedicated efforts of many people who are not listed as authors. Their contributions are acknowledged with great appreciation. The experiment was made possible by the inventiveness and the diligent efforts of the HERA machine group. The strong support and encouragement of the DESY directorate have been invaluable.

References

1. PLUTO Coll., C. Berger et al., Nucl. Phys. B **281**, 365 (1987)
2. M. Krawczyk, A. Zembrzuski, M. Staszel (Warsaw U.), Phys. Rept. **345**, 265 (2001)
3. E.D. Bloom et al., Phys. Rev. Lett. **23**, 930 (1969)
4. M. Breidenbach et al., Phys. Rev. Lett. **23**, 935 (1969)
5. J.I. Friedman, H.W. Kendall, Ann. Rev. Nucl. Sci. **22**, 203 (1972)
6. H1 Coll., C. Adloff et al., Eur. Phys. J. C **13**, 397 (2000)
7. H1 Coll., A. Aktas et al.. Hep-ex/0401010
8. ZEUS Coll., J. Breitweg et al., Phys. Lett. B **479**, 37 (2000)
9. C.H. Llewellyn Smith, Phys. Lett. B **79**, 83 (1978)
10. I. Kang, C.H. Llewellyn Smith, Nucl. Phys. B **166**, 413 (1980)
11. J.F. Owens, Phys. Rev. D **21**, 54 (1980)
12. M. Fontannaz, A. Mantrach, D. Schiff, Z. Phys. C **6**, 241 (1980)
13. W.J. Stirling, Z. Kunszt, Proc. HERA Workshop, R. Peccei (ed.), Vol. 1, p. 331. DESY (1987)
14. M. Drees, F. Halzen, Phys. Rev. Lett. **61**, 275 (1988)
15. M. Drees, R.M. Godbole, Phys. Rev. Lett. **61**, 682 (1988)
16. M. Drees, R.M. Godbole, Phys. Rev. Lett. **39**, 169 (1989)
17. H. Baer, J. Ohnemus, J.F. Owens, Z. Phys. C **42**, 657 (1989)
18. H. Baer, J. Ohnemus, J.F. Owens, Phys. Rev. D **40**, 2844 (1989)
19. ZEUS Coll., M. Derrick et al., Phys. Lett. B **322**, 287 (1994)
20. ZEUS Coll., M. Derrick et al., Phys. Lett. B **348**, 665 (1995)
21. D. Graudenz, Preprint hep-ph/9710244, 1997
22. S. Catani, M.H. Seymour, Nucl. Phys. B **485**, 291 (1997)
23. S. Frixione, Z. Kunszt, A. Signer, Nucl. Phys. B **467**, 399 (1996)
24. S. Frixione, Nucl. Phys. B **507**, 295 (1997)
25. S. Frixione, G. Ridolfi, Nucl. Phys. B **507**, 315 (1997)
26. ZEUS Coll., U. Holm (ed.), The ZEUS Detector. Status Report (unpublished), DESY (1993), available on http://www-zeus.desy.de/bluebook/bluebook.html
27. N. Harnew et al., Nucl. Inst. Meth. A **279**, 290 (1989)
28. B. Foster et al., Nucl. Phys. Proc. Suppl. B **32**, 181 (1993)
29. B. Foster et al., Nucl. Inst. Meth. A **338**, 254 (1994)
30. M. Derrick et al., Nucl. Inst. Meth. A **309**, 77 (1991)
31. A. Andresen et al., Nucl. Inst. Meth. A **309**, 101 (1991)
32. A. Caldwell et al., Nucl. Inst. Meth. A **321**, 356 (1992)
33. A. Bernstein et al., Nucl. Inst. Meth. A **336**, 23 (1993)
34. ZEUS Coll., J. Breitweg et al., Phys. Lett. B **407**, 432 (1997)
35. J. Andruszków et al., Preprint DESY-92-066, DESY, 1992
36. ZEUS Coll., M. Derrick et al., Z. Phys. C **63**, 391 (1994)
37. J. Andruszków et al., Acta Phys. Pol. B **32**, 2025 (2001)
38. G.A. Schuler, T. Sjöstrand, Phys. Lett. B **376**, 193 (1996)
39. M. Drees, R.M. Godbole, Phys. Rev. D **50**, 3124 (1994)
40. T. Uematsu, T. Walsh, Phys. Lett. B **101**, 263 (1981)
41. T. Uematsu, T. Walsh, Nucl. Phys. B **199**, 93 (1982)
42. F. Borzumati, G. Schuler, Z. Phys. C **58**, 139 (1993)
43. M. Glück, E. Reya, I. Schienbein, Phys. Rev. D **60**, 054019 (1999)
44. M. Glück, E. Reya, M. Stratmann, Phys. Rev. D **54**, 5515 (1996)
45. D. de Florian, C. Canal, R. Sassot, Z. Phys. C **75**, 265 (1997)
46. M. Klasen, G. Kramer, B. Pötter, Eur. Phys. J. C **1**, 261 (1998)
47. M. Glück, E. Reya, M. Stratmann, Phys. Rev. D **51**, 3220 (1995)
48. S. Catani et al., Nucl. Phys. B **406**, 187 (1993)
49. S.D. Ellis, D.E. Soper, Phys. Rev. D **48**, 3160 (1993)
50. ZEUS Coll., J. Breitweg et al., Eur. Phys. J. C **1**, 109 (1998)
51. H. Abramowicz, A. Caldwell, R. Sinkus, Nucl. Inst. Meth. A **365**, 508 (1995)
52. G.M. Briskin, Ph.D. Thesis, Tel Aviv University, 1998 (Unpublished)

53. ZEUS Coll., J. Breitweg et al., Eur. Phys. J. C **11**, 35 (1999)
54. ZEUS Coll., S. Chekanov et al., Eur. Phys. J. C **23**, 615 (2002)
55. F. Jacquet, A. Blondel, Proceedings of the Study for an *ep* Facility for Europe, U. Amaldi (ed.), p. 391. Hamburg, Germany (1979). Also in preprint DESY 79/48
56. G. Marchesini et al., Comput. Phys. Commun. **67**, 465 (1992)
57. T. Sjöstrand et al., Comput. Phys. Commun. **135**, 238 (2001)
58. M. Glück, E. Reya, A. Vogt, Phys. Rev. D **46**, 1973 (1992)
59. A.D. Martin, R.G. Roberts, W.J. Stirling, Phys. Rev. D **50**, 6734 (1994)
60. CTEQ Coll., H.L. Lai et al., Eur. Phys. J. C **12**, 375 (2000)
61. B. R. Webber, Nucl. Phys. B **238**, 492 (1984)
62. B. Andersson et al., Phys. Rep. **97**, 31 (1983)
63. R. Brun et al., GEANT3, Technical Report CERN-DD/EE/84-1, CERN, 1987
64. R.K. Ellis, D.A. Ross, A.E. Terrano, Nucl. Phys. B **178**, 421 (1981)
65. B.W. Harris, J.F. Owens, Phys. Rev. D **56**, 4007 (1997)
66. B.W. Harris, J.F. Owens, Phys. Rev. D **57**, 5555 (1998)
67. M. Klasen, G. Kramer, Z. Phys. C **76**, 67 (1997)
68. M. Klasen, T. Kleinwort, G. Kramer, Eur. Phys. J. direct C **1**, 1 (1998)
69. P. Aurenche et al., Eur. Phys. J. C **17**, 413 (2000)
70. B.W. Harris, M. Klasen, J. Vossebeld, Proc. Workshop on Monte Carlo Generators for HERA Physics, T.A. Doyle et al. (ed.), p. 171. DESY, Hamburg, Germany (1999). Also in preprint DESY-PROC-1999-02 (hep-ph/9905348), available on http://www.desy.de/~heramc/
71. P. Aurenche, J.P. Guillet, M. Fontannaz, Z. Phys. C **64**, 621 (1994)
72. A. Kwiatkowski, H. Spiesberger, H.-J. Möhring, Comput. Phys. Commun. **69**, 155 (1992)
73. H. Spiesberger, An Event Generator for *ep* Interactions at HERA Including Radiative Processes (Version 4.6), 1996, available on http://www.desy.de/~hspiesb/heracles.html
74. S. Bentvelsen, J. Engelen, P. Kooijman, Proc. Workshop on Physics at HERA, W. Buchmüller, G. Ingelman (eds.), Vol. 1, p. 23. Hamburg, Germany, DESY (1992)
75. H. Spiesberger, HERACLES, DJANGOH: Event Generation for *ep* Interactions at HERA Including Radiative Processes, 1998, available on http://www.desy.de/~hspiesb/djangoh.html
76. K. Charchula, G.A. Schuler, H. Spiesberger, Comput. Phys. Commun. **81**, 381 (1994)
77. Y. Azimov et al., Phys. Lett. B **165**, 147 (1985)
78. G. Gustafson, Phys. Lett. B **175**, 453 (1986)
79. G. Gustafson, U. Pettersson, Nucl. Phys. B **306**, 746 (1988)
80. B. Andersson, G. Gustafson, L. Lönnblad, Z. Phys. C **43**, 625 (1989)
81. L. Lönnblad, Comput. Phys. Commun. **71**, 15 (1992)
82. G. Ingelman, A. Edin, J. Rathsman, Comput. Phys. Commun. **101**, 108 (1997)
83. G. Corcella, I.G. Knowles, G. Marchesini, S. Moretti, K. Odagiri, P. Richardson, M.H. Seymour, B.R. Webber, JHEP **0101**, 010 (2001)
84. J.M. Butterworth, S. Butterworth, Comput. Phys. Commun. **153**, 164 (2003)
85. ZEUS Coll., S. Chekanov et al., Phys. Lett. B **560**, 7 (2003)